Time-Resolved Spectral Diffusion of a Multimode Mechanical Memory

Fiaschi, Niccolò; Scarpelli, Lorenzo; Korsch, Alexander Rolf; Zivari, Amirparsa; Gröblacher, Simon

DOI
10.1103/tcpy-jhjy

Publication date
2025

Document Version
Final published version

Published in
Physical review letters

Citation (APA)
Fiaschi, N., Scarpelli, L., Korsch, A. R., Zivari, A., & Gröblacher, S. (2025). Time-Resolved Spectral Diffusion of a Multimode Mechanical Memory. *Physical review letters*, *134*(24), Article 243604. https://doi.org/10.1103/tcpy-jhjy

Time-Resolved Spectral Diffusion of a Multimode Mechanical Memory

Niccolò Fiaschi,[1,*] Lorenzo Scarpelli,[1] Alexander Rolf Korsch,[2,3,1] Amirparsa Zivari,[1] and Simon Gröblacher[1,†]
[1]Kavli Institute of Nanoscience, Department of Quantum Nanoscience, Delft University of Technology, 2628CJ Delft, The Netherlands
[2]Department of Physics, Fudan University, Shanghai 200433, People's Republic of China
[3]Department of Physics, School of Science, Westlake University, Hangzhou 310030, People's Republic of China

(Received 24 January 2025; accepted 27 May 2025; published 20 June 2025)

High-frequency phonons hold great promise as carriers of quantum information on chip and as quantum memories. Because of their coherent interaction with several systems, their compact mode volume, and slow group velocity, multiple experiments have recently demonstrated coherent transport of information on chip using phonon modes, interconnecting distinct quantum devices. Strongly confined phonons in waveguidelike geometries are particularly interesting because of their long lifetime. However, spectral diffusion has been observed to substantially limit their coherence times [S. M. Meenehan *et al.*, Silicon optomechanical crystal resonator at millikelvin temperatures, Phys. Rev. A **90**, 011803(R) (2014), A. Wallucks *et al.*, A quantum memory at telecom wavelengths, Nat. Phys. **16**, 772 (2020), and G. S. MacCabe *et al.*, Nano-acoustic resonator with ultralong phonon lifetime, Science **370**, 840 (2020)]. Coupling to two-level systems is suspected to be a major contributor to the diffusion; however, to date, the origin and underlying mechanisms are still not fully understood. Here, we perform a time-domain study on two adjacent mechanical modes (separated by around 5 MHz) and show that the frequency positions of the two modes are not correlated in time, in agreement with our theoretical model and Monte Carlo simulations. This result is an important step in fully understanding the microscopic mechanisms of dephasing in mechanical quantum buses and memories.

DOI: 10.1103/tcpy-jhjy

Introduction—Over the past years, several ground-breaking experiments have shown that high-frequency phonons can be effectively used as carriers of quantum information on chip. In particular, surface acoustic waves (SAWs) have enabled quantum state transfer and remote entanglement between two superconducting qubits [1]. SAWs have received most of the early interest, since they represent a mature platform for coherent control of quantum information on chip, having also allowed one to realize a beam splitter [2] and a phase shifter [3]. However, SAWs have inherently limited coherence time due to their short lifetime on the order of microseconds [4]. More strongly confined phonons in waveguidelike systems are a promising alternative to overcoming these limitations and allow for on-chip distribution of quantum information [5,6]. In this type of system, the coherence of the information that travels in the waveguide is ultimately limited by the spectral diffusion, i.e., the frequency jitter of the mechanical mode. This phenomenon was initially observed and studied in single-mode optomechanical cavities [7], where the coherence time of the single mechanical mode is on the order of 100 μs [8,9]. The generally accepted interpretation of this phenomenon involves a bath of two-level systems (TLS) that interact with the mechanical mode(s) [7,9]. Similar types of defects are widely studied in superconducting circuits, since they are a major source of energy loss and decoherence [10–13]. Engineering the phononic environment that interacts with the TLS can be used to investigate and control the TLS [14,15]. While their actual nature remains elusive, efforts in understanding the microscopic characteristics of these TLS are ongoing [16].

In this work, we take a new approach to studying the time dynamics of the spectral diffusion of two spectrally close mechanical modes (centered at ∼5 GHz and spaced by ∼5 MHz) of the same optomechanical device, with a time resolution of a few microseconds. We find that the frequency positions of the two mechanical modes are not correlated in time. Even with the measurements operating in a continuous fashion, leading to an effective thermal bath elevated from the 50 mK environment, our result helps in understanding the effect of TLSs on mechanical resonators, developing a method for fast time resolution of TLS-induced frequency shifts. To support our findings and for a better understanding of the TLS to mechanical mode interaction, we further develop a theoretical model and perform Monte Carlo simulations of the frequency shift—in good qualitative agreement with the measured data. The model confirms the coupling mechanism, strength, and TLSs spectral distribution. The developed method can help the design of mechanical systems, providing a tool to estimate the spectral diffusion for any mechanical mode.

*Contact author: nfiaschi@berkeley.edu
†Contact author: s.groeblacher@tudelft.nl

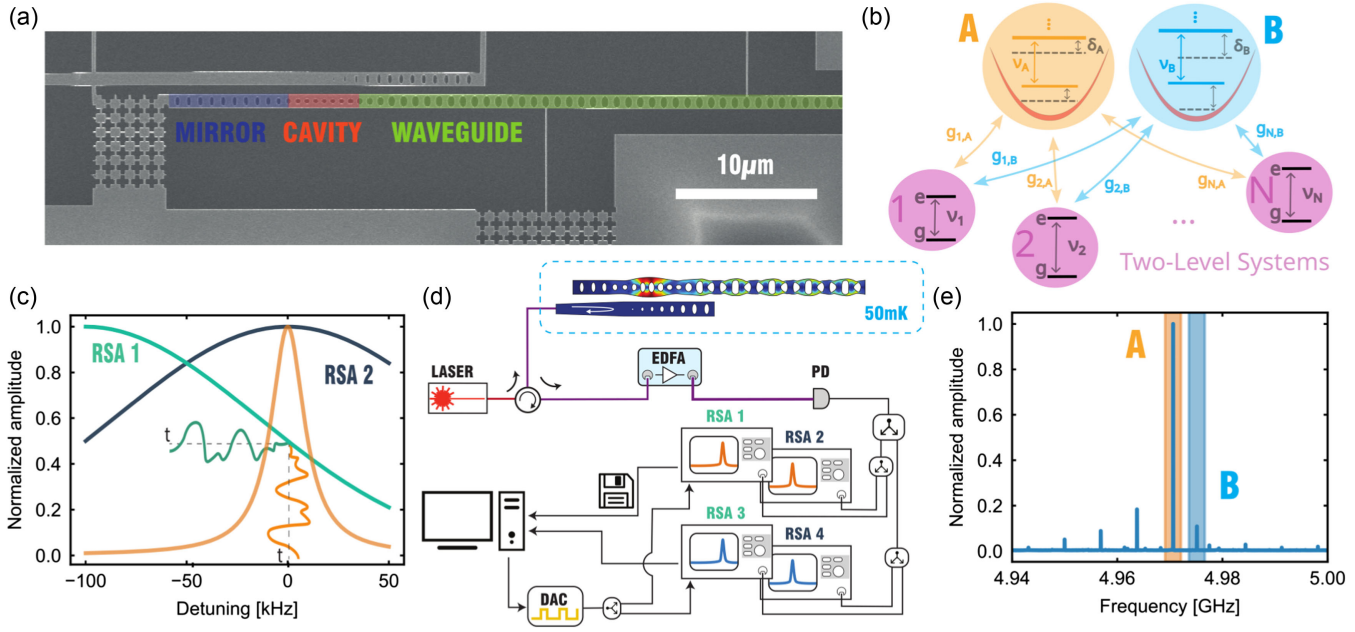

FIG. 1. Setup and device characterization. (a) SEM image of a device nominally identical to the one used in the measurements. The optomechanical cavity is highlighted in red, the photonic and phononic mirror in blue, and the single-mode (for in-plane symmetric modes) mechanical waveguide (and photonic mirror) in green. The total length of the waveguide ∼200 μm. (b) Schematic of the theoretical model for the Monte Carlo simulations. The mechanical modes A and B at frequency ν_A and ν_B are coupled to a bath of N TLS. Each TLS has frequency ν_i and coupling rate $g_{i,A}$ and $g_{i,B}$, with i being the index of the TLS, to mode A and B, respectively. Note that the coupling rate for the two modes is, in general, different for each TLS. The bath shifts the frequency of mode A by δ_A and of B by δ_B. (c) Sketch of the method used for resolving the spectral diffusion of a single-mode mechanical mode in time (orange line, averaged PSD). See the text for details. (d) Scheme of the experimental setup. The laser is routed to the device at the base plate of the dilution refrigerator via a fiber circulator and a lensed fiber. The light coming out of the device is amplified with an erbium-doped fiber amplifier (EDFA) and sent to a fast photodiode. The signal from the photodiode is split with rf splitters and analyzed with four synchronized real-time spectrum analyzers (RSA1–4). All RSAs are triggered externally via a TTL signal from a DAC card, which allows submicrosecond synchronization. (e) Mechanical spectrum of the device with several visible modes. The modes measured in this Letter are called mode A (shaded in orange) and mode B (shaded in blue).

Methods—The device used in this work, identical to the one of [5], consists of an optomechanical cavity coupled to a phononic waveguide, where the freestanding end acts as a mechanical mirror. The hybridized mechanical modes of the structure form a series of Fabry-Pérot modes, with similar spatial profile, closely spaced by ∼5 MHz around a central frequency of ∼5 GHz. The optical cavity features a single mode for the optical field with a resonance in the telecom band around ∼1550 nm. Figure 1(a) shows a scanning electron microscope (SEM) image of a device nominally identical to the one used in this work. We model our system as two mechanical modes of the cavity-waveguide system (modes A and B), which are dispersively coupled to a bath of TLS. The dispersive coupling results in a frequency shift of the mechanical modes, which depends on the instantaneous occupation, coupling strength, and detuning of the TLS to that particular mode. Differences in coupling strengths and detunings for the two modes result in different frequency shifts and lead to uncorrelated frequency jitters [see Fig. 1(b) for a schematic of the model and Supplemental Material, Sec. 9 [17], for more details).

To resolve the mechanical frequency of the device in time, we use a frequency demodulation scheme, with its main working principle illustrated in Fig. 1(c). For each mode, we first measure its power spectral density (PSD) and average it over several scans (orange curve). We then use two real-time spectrum analyzers (RSAs) in zero-span mode to acquire the total power filtered from the resolution bandwidth (RBW) filter as a function of time. One RSA (RSA1, with RBW depicted by the green line in the figure) has the filter detuned by $-\mathrm{RBW}/2 = -100$ kHz from the mechanical mode. In this way, the frequency jitter is mapped onto an amplitude modulation of the signal measured by RSA1. The dark orange line depicts a sketch of the time trace of the frequency jitter, while the dark green line is the corresponding amplitude variation of the signal measured (and the dashed lines are the time axes). As the measured power is also proportional to the thermal mechanical population, a change in the amplitude of the mechanical peak will also cause a change in the amplitude of the measured signal. For this reason, the second RSA (RSA2, RBW in dark gray) has the filter on resonance with the mechanical mode, such that its sensitivity to the

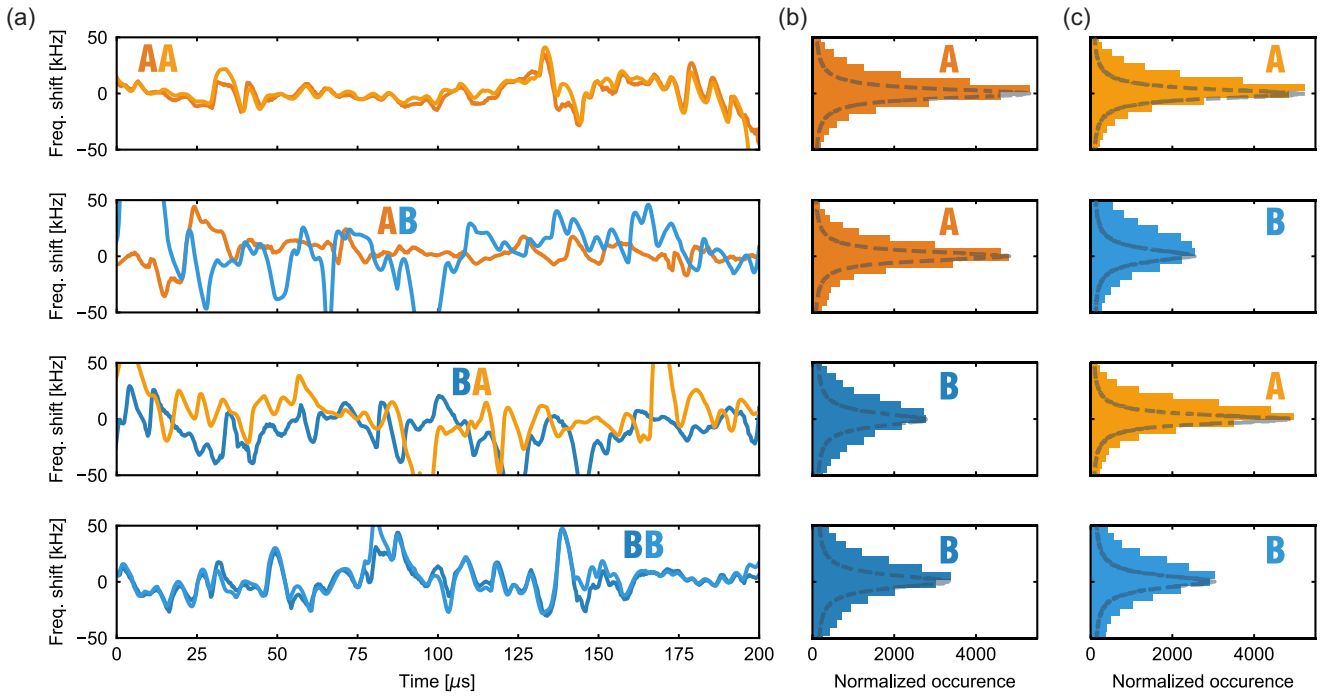

FIG. 2. Frequency jitter in time. (a) Time traces for mode A (orange measured on RSA1 and light orange on RSA3) and B (blue measured on RSA1 and light blue on RSA3). From top to bottom: the synchronized measurements are for the configurations AA, AB, BA, and BB measured from RSA1 and RSA3, respectively (using RSA2 and RSA4 for the amplitude normalization). AA and BB have clearly (almost) identical time traces, while AB and BA show uncorrelated time traces. (b),(c) Histogram of the frequency shift modes AA, AB, BA, and BB (from top to bottom) for a trace with 10 ms length. The dashed black line is the averaged mechanical spectrum (independently) measured with the corresponding RSA, which is in good agreement with the histogram. All data here are measured at 50 mK.

frequency jitter is negligible. In this way, we can measure the amplitude fluctuations of the signal with RSA2 and the amplitude and frequency fluctuations with RSA1. Normalizing the signal from RSA1 with the one from RSA2 then allows us to extract the frequency position of the mechanical mode in time, even if the signal is modulated in amplitude and frequency. We use two RSAs in this configuration for each mechanical mode in all the measurements.

The setup for the frequency demodulation is schematically shown in Fig. 1(d). A continuous wave (cw) laser, red detuned from the optical resonance by the average mechanical frequency of the modes of interest (≈5 GHz), is routed to the device at the mixing chamber of a dilution refrigerator (temperature of around 50 mK) via a circulator and a lensed fiber (coupling efficiency of 10%). The cw light is partially absorbed by the device, creating a thermal population in the mechanical modes of interest. This population is read via the beam-splitter interaction with the same cw laser, which creates sidebands detuned from the laser carrier by the mechanical frequencies [5]. Throughout all measurements, the instantaneous photon number in the optomechanical cavity is approximately 3000 (see Supplemental Material, Sec. 1 [17], for more information). The output of the circulator is amplified with an erbium-doped fiber amplifier (EDFA) to boost the signal on a fast photodetector. The output of the detector is split with three power splitters and sent to four RSAs (1–4). RSA1 and 3 are detuned by $-\mathrm{RBW}/2 = -100$ kHz from the measured mechanical mode, while RSA2 and 4 are always on resonance with them. The RSAs are synchronized in the data acquisition via a transistor-transistor logic (TTL) signal that triggers all the RSAs simultaneously, with a relative delay of submicroseconds.

After the scan of the optical resonance (cf. Supplemental Material, Sec. 1 [17]), we measure the PSD of the device over a broad range of frequencies to identify the two mechanical modes of interest, which is plotted in Fig. 1(e). We see that the device has a comb of mechanical modes due to the hybridization of the single-mode mechanical cavity with the Fabry-Pérot cavity formed by the long waveguide with its freestanding end [5]. The shaded regions in the plot highlight the two modes used in this work. The resonances have a FWHM = 20 kHz (see Supplemental Material, Sec. 1 [17], for details). We use optomechanical-induced transparency to determine the optomechanical coupling of each mode, finding 0.3 MHz for A and 0.2 MHz for B. We also measure a phonon lifetime of around 1 ms (see Supplemental Material, Sec. 2 [17]).

For an initial characterization of the frequency diffusion, we use RSA1 and RSA3 to take synchronized fast frequency scans of the peaks (PSD), similar to the procedure reported in [8]. To obtain sufficient information of the peak, the fastest possible scan takes 200 μs (RBW = 10 kHz). In this configuration, approximately half of the scans have more than one prominent peak (see Supplemental Material, Sec. 3 [17]). This indicates that the timescale of the jitter is much faster than the scanning time. We overcome this limitation by using a frequency demodulation scheme, which allows us to use larger RBW and, therefore, have finer time resolution.

Results—We use the four RSAs to measure (synchronized) time traces of the two mechanical modes in four configurations: *AA*, *AB*, *BA*, and *BB*. RSA1 (3) is detuned by $-\mathrm{RBW}/2 = -100$ kHz from the mode *A* (*A*), *A* (*B*), *B* (*A*), and *B* (*B*), respectively, while RSA2 and 4 are always on resonance with the mode measured by RSA1 and 3, respectively. Each time trace is 10 ms long. For this measurement, the choice of the RBW is crucial: We set a 200 kHz RBW filter as a trade-off for having a large enough time resolution ($\sim 1/\mathrm{RBW} = 5$ μs) while still maintaining a good signal-to-noise ratio, high dynamical range, and high sensitivity. The RBW is also chosen to be much bigger than the average frequency shift to avoid signal distortion. We report an average signal-to-noise ratio of 10 for mode *A* (with a maximum value of 80) and 5 for *B* (with a maximum value of 30). The peak fluctuates in the linear part (in the detuned case) and on the flat part (in the resonant case) of the filter. For the chosen filter, a typical frequency fluctuation of 10 kHz (FWHM/2) gives a 0.7% relative change in amplitude for the filter at resonance with the mechanical mode and a 7% relative change for the filter detuned by $-\mathrm{RBW}/2$. With the amplitude of the signal from RSA2 and 4, we normalize the trace measured from RSA1 and 3 (see Supplemental Material, Sec. 6 [17]). We then use the filter shape to convert the amplitude fluctuations into frequency fluctuations (see Supplemental Material, Sec. 5 [17]). The result of the measurements is reported in Fig. 2(a), where we plot the frequency shift in time, from top to bottom, for the four configurations *AA*, *AB*, *BA*, and *BB*, in orange (blue) and light orange (light blue) for mode *A* (*B*). In this plot, we show a 200-μs-long segment of the measured trace. It is clearly visible that the *AA* and *BB* configurations have highly correlated traces, while the *AB* and *BA* configurations have uncorrelated time traces of the two modes. The (common mode) frequency jitter, which can be caused by laser frequency shifts and changes in laser power, is much smaller than the measured frequency shifts (see Supplemental Material, Sec. 4 [17]). We further show in Figs. 2(b) and 2(c) the histogram of the frequency shift for the complete time traces. The letters in the plot refer to which mode is analyzed. The dashed black line is the mechanical PSD as measured from the RSAs in scanning mode (averaging for approximately 30 s for each measurement). Note that the two (independent) measurements are in very good agreement, confirming the validity of the method used. The small discrepancy in the FWHM of the distribution should arise mainly from the noise in the measurement of the amplitude from RSA2 and 4. The small discrepancy in the center of the distribution is attributed to slow frequency drifts of the mechanical modes [8].

To quantitatively assess if the time traces are correlated or not, we calculate the correlation function in the four configurations (see Supplemental Material, Sec. 7 [17,18]), and we show the results for zero delay ($\tau = 0$) in Fig. 3. It is clearly visible from the matrix that *AA* and *BB* have a strong correlation, while *AB* and *BA* have uncorrelated values. We would like to note that a more detailed study with different RBWs could be beneficial in extracting short-delay coherence time. To validate the measurements and gain some additional information on the frequency jitter mechanism, we develop a theoretical model and use it to run Monte Carlo simulations to obtain the frequency diffusion of two mechanical modes shifted by a bath of TLS (see Supplemental Material, Sec. 9 [17]). For our model, we use a COMSOL simulation to calculate the coupling rates between the mechanical modes of the device and each TLS of the bath. We find that each mechanical mode can couple very differently to the same TLS bath. We then calculate, for each time step of the simulation, the frequency shift of the mechanical mode arising from the dispersive coupling with each TLS. We find good qualitative agreement between the measured data and the model, finding a frequency jitter in time with amplitude and timescale comparable with the one measured and with the same pattern of correlation, as can be seen in Fig. 2(a) and Supplemental Material, Sec. 9 [17], Fig. 8(d), and Fig. 3 and Supplemental Material, Sec. 9 [17], Fig. 9.

In order to get a better understanding of the nature of the TLS, we perform the same experiment at a temperature of 800 mK (see Supplemental Material, Sec. 8 [17]) and perform Monte Carlo simulations up to 4K (see Supplemental Material, Sec. 9 [17]), and in both cases the correlation results are practically identical. This indicates that a considerable part of the frequency diffusion is caused by far-detuned TLS, which are only partially affected by the higher temperature [9], as the TLS with frequency close to the mechanical modes of interest are mostly saturated.

Discussion—In our experiment, we show that two mechanical modes, even if spectrally close and with similar mode shapes, have an uncorrelated spectral diffusion for timescales greater than a few microseconds. This leads us to conclude that when using two devices in a dual-rail scheme [19,25] or a single device with multiple mechanical modes [6] the resulting coherence times would be similar. The uncorrelated traces and the developed model show that the two modes are coupled very differently to the same surface defect (TLS) bath, which, most likely, are the cause

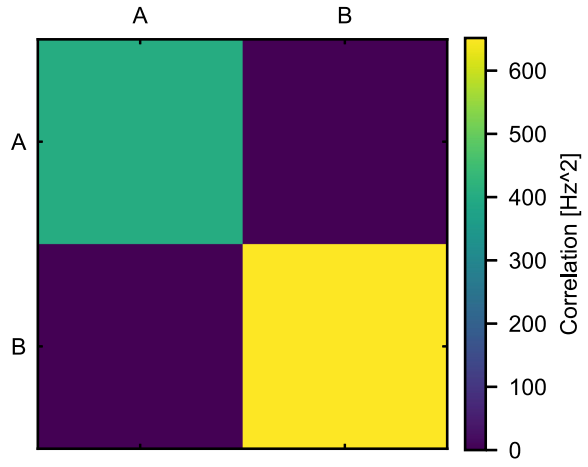

FIG. 3. Correlation of the frequency jitter. Correlation for zero delay ($\tau = 0$, as defined in Supplemental Material, Sec. 7 [17,18]) for the mechanical mode configurations *AA*, *AB*, *BA*, and *BB* using the full traces of Fig. 2 with 10 ms length. The *AA* and *BB* combinations show strong correlations, while the *AB* and *BA* combinations are uncorrelated. All data here are measured at 50 mK.

of the jittering [9]. From the model, we estimate that each TLS can have a difference in coupling rate to the two mechanical modes of up to 2 orders of magnitude. Our results shed further light on the cause of the frequency diffusion in mechanical oscillators and could be used to design higher coherence-time multimode devices (that have mostly common mode frequency shift, for example). Additional experiments are, however, required to fully understand the underlying mechanisms and to open the way to long coherence-time mechanical quantum memories without the use of dynamical decoupling methods. In particular, a detailed and systematic analysis via surface treatments of the silicon is necessary or the use of alternative materials such as GaP or silicon nitride. We can further conclude that, in order to reach long coherence times in mechanical quantum memories, it is necessary to saturate the TLS over a very wide frequency range ($\gtrsim$20 GHz), for example, through an ac electric field. For this reason, the use of acoustic metamaterials—phononic shields—given their limited band gap (~2 GHz), have been only partially beneficial for the coherence time [8,9].

Acknowledgments—We thank Robert Stockill and Raymond Schouten for valuable discussions and Clinton Potts for support. We further acknowledge assistance from the Kavli Nanolab Delft. This work is financially supported by the European Research Council (ERC CoG Q-ECHOS, 101001005) and is part of the research program of the Netherlands Organization for Scientific Research (NWO), supported by the NWO Frontiers of Nanoscience program, as well as through a Vrij Programma (680-92-18-04) grant.

N. F. devised and planned the experiment, built the setup, and performed the measurements, with help from A. R. K. A. Z. fabricated the device. N. F., L. S., and S. G. analyzed the data and wrote the manuscript. S. G. supervised the project.

The authors declare no competing interests.

Data availability—The data that support the findings of this Letter are openly available [26].

[1] A. Bienfait, K. J. Satzinger, Y. P. Zhong, H.-S. Chang, M.-H. Chou, C. R. Conner, E. Dumur, J. Grebel, G. A. Peairs, R. G. Povey, and A. N. Cleland, Phonon-mediated quantum state transfer and remote qubit entanglement, Science **364**, 368 (2019).

[2] H. Qiao, É. Dumur, G. Andersson, H. Yan, M.-H. Chou, J. Grebel, C. R. Conner, Y. J. Joshi, J. M. Miller, R. G. Povey, X. Wu, and A. N. Cleland, Splitting phonons: Building a platform for linear mechanical quantum computing, Science **380**, 1030 (2023).

[3] L. Shao, D. Zhu, M. Colangelo, D. Lee, N. Sinclair, Y. Hu, P. T. Rakich, K. Lai, K. K. Berggren, and M. Lončar, Electrical control of surface acoustic waves, Nat. Electron. **5**, 348 (2022).

[4] G. Andersson, A. L. O. Bilobran, M. Scigliuzzo, M. M. de Lima, J. H. Cole, and P. Delsing, Acoustic spectral hole-burning in a two-level system ensemble, npj Quantum Inf. **7**, 15 (2021).

[5] A. Zivari, R. Stockill, N. Fiaschi, and S. Gröblacher, Non-classical mechanical states guided in a phononic waveguide, Nat. Phys. **18**, 789 (2022).

[6] A. Zivari, N. Fiaschi, R. Burgwal, E. Verhagen, R. Stockill, and S. Gröblacher, On-chip distribution of quantum information using traveling phonons, Sci. Adv. **8**, eadd2811 (2022).

[7] S. M. Meenehan, J. D. Cohen, S. Gröblacher, J. T. Hill, A. H. Safavi-Naeini, M. Aspelmeyer, and O. Painter, Silicon optomechanical crystal resonator at millikelvin temperatures, Phys. Rev. A **90**, 011803(R) (2014).

[8] A. Wallucks, I. Marinković, B. Hensen, R. Stockill, and S. Gröblacher, A quantum memory at telecom wavelengths, Nat. Phys. **16**, 772 (2020).

[9] G. S. MacCabe, H. Ren, J. Luo, J. D. Cohen, H. Zhou, A. Sipahigil, M. Mirhosseini, and O. Painter, Nano-acoustic resonator with ultralong phonon lifetime, Science **370**, 840 (2020).

[10] P. V. Klimov *et al.*, Fluctuations of energy-relaxation times in superconducting qubits, Phys. Rev. Lett. **121**, 090502 (2018).

[11] S. Mittal, K. Adachi, N. Frattini, M. Urmey, S.-X. Lin, A. Emser, C. Metzger, L. Talamo, S. Dickson, D. Carlson, S. Papp, C. Regal, and K. Lehnert, Annealing reduces Si_3N_4 microwave-frequency dielectric loss in superconducting resonators, Phys. Rev. Appl. **21**, 054044 (2024).

[12] A. Bozkurt, H. Zhao, C. Joshi, H. G. LeDuc, P. K. Day, and M. Mirhosseini, A quantum electromechanical interface for long-lived phonons, Nat. Phys. **19**, 1326 (2023).

[13] Z.-H. Zhang, K. Godeneli, J. He, M. Odeh, H. Zhou, S. Meesala, and A. Sipahigil, Acceptor-induced bulk dielectric loss in superconducting circuits on silicon, Phys. Rev. X **14**, 041022 (2024).
[14] M. Chen, J. C. Owens, H. Putterman, M. Schäfer, and O. Painter, Phonon engineering of atomic-scale defects in superconducting quantum circuits, Sci. Adv. **10**, eado6240 (2024).
[15] M. Odeh, K. Godeneli, E. Li, R. Tangirala, H. Zhou, X. Zhang, Z.-H. Zhang, and A. Sipahigil, Non-Markovian dynamics of a superconducting qubit in a phononic bandgap, Nat. Phys. **21**, 406 (2025).
[16] C. Müller, J. H. Cole, and J. Lisenfeld, Towards understanding two-level-systems in amorphous solids: Insights from quantum circuits, Rep. Prog. Phys. **82**, 124501 (2019).
[17] See Supplemental Material at http://link.aps.org/supplemental/10.1103/tcpy-jhjy, for additional data and simulations (including Refs. [5,7,9,18–24]).
[18] R. Kubo, A stochastic theory of line shape, in *Advances in Chemical Physics* (John Wiley and Sons, Ltd, New York, 1969), pp. 101–127.
[19] N. Fiaschi, B. Hensen, A. Wallucks, R. Benevides, J. Li, T. P. M. Alegre, and S. Gröblacher, Optomechanical quantum teleportation, Nat. Photonics **15**, 817 (2021).
[20] M. Aspelmeyer, T. J. Kippenberg, and F. Marquardt, Cavity optomechanics, Rev. Mod. Phys. **86**, 1391 (2014).
[21] K. Cui, Z. Huang, N. Wu, Q. Xu, F. Pan, J. Xiong, X. Feng, F. Liu, W. Zhang, and Y. Huang, Phonon lasing in a hetero optomechanical crystal cavity, Photonics Res. **9**, 937 (2021).
[22] W. A. Phillips, Two-level states in glasses, Rep. Prog. Phys. **50**, 1657 (1987).
[23] A. Y. Cleland, E. A. Wollack, and A. H. Safavi-Naeini, Studying phonon coherence with a quantum sensor, Nat. Commun. **15**, 4979 (2024).
[24] A. Berthelot, I. Favero, G. Cassabois, C. Voisin, C. Delalande, P. Roussignol, R. Ferreira, and J. M. Gérard, Unconventional motional narrowing in the optical spectrum of a semiconductor quantum dot, Nat. Phys. **2**, 759 (2006).
[25] R. Riedinger, A. Wallucks, I. Marinković, C. Löschnauer, M. Aspelmeyer, S. Hong, and S. Gröblacher, Remote quantum entanglement between two micromechanical oscillators, Nature (London) **556**, 473 (2018).
[26] N. Fiaschi, L. Scarpelli, A. R. Korsch, A. Zivari, and S. Groeblacher, Data from: Time-resolved spectral diffusion of a multimode mechanical memory, 10.5281/zenodo.15584323 (2025).